J. Webster (ed.), *Wiley Encyclopedia of Electrical and Electronics Engineering*

THERAPEUTIC ULTRASOUND

Ultrasonic waves in the frequency range of 500 kHz to 10 MHz have been investigated for use in various therapeutic applications such as hyperthermia (1), rapid hyperthermia (2), thermal surgery (3, 4), and drug activation (5, 6). Experimental evidence gathered over the last five decades by several independent research groups suggests that high-intensity focused ultrasound (HIFU) continues to hold promise in applications where deep localized targeting of diseased tissue is required. HIFU is the only known form of nonionizing radiation suitable for deep penetration (up to 15 cm) with millimeter-size focal spots. For example, even with the use of phased arrays, therapeutic microwave heating appears to be limited to superficial tumor sites (7). In addition, methods and materials for the generation and control of ultrasound power deposition patterns are inexpensive compared to other energy-based therapeutic modalities. Most significantly, the safety concerns with ultrasound are minimal when properly designed and characterized equipment and transducers are used. Therefore, HIFU is a very promising therapeutic modality with little or no risk when properly used.

Even though the therapeutic applications of HIFU have been investigated by numerous groups for a long time, it is safe to say that there has never been any period where research in this area has been more active than the last decade. This is due to significant advances in a number of enabling technologies that will eventually move HIFU systems from the laboratory to the clinic. The most significant of these technologies are:

(1) Advances in a number of diagnostic imaging modalities that could be used in guidance, monitoring, and control of HIFU noninvasively or with minimal invasiveness.
(2) Advances in transducer materials and fabrication technologies that offer the promise of reliable and inexpensive applicator systems in clinical applications.
(3) Advances in multielement and phased array technologies, including optimal methods for pattern synthesis. Phased arrays will increase the flexibility of applicator systems and may make it possible to noninvasively treat targets previously considered unreachable by ultrasound, for example, liver tumors that are partially obstructed by the rib cage (8).

In addition to the above technological advances, significant progress that led to a better understanding of the modes of interaction of HIFU with tissue occurred in the 1970s and early 1980s. Among the more significant results in this regard are:

(1) Understanding of thermal and mechanical tissue damage mechanisms due to HIFU. In particular, thresholds for thermal and mechanical tissue damage for various *in vivo* mammalian tissues with clinical relevance were measured and published.
(2) The emergence of several quantitative measures of tissue damage due to thermal effects, based on experimental and physiological evidence. Today, the concept of *equivalent minutes at* $43^{\circ}C$ as a measure of *thermal dose*, introduced by Saparato and Dewey (9) for characterizing hyperthermia, appears to be the

leading measure. Recently, Hynynen and coworkers (10) have used this concept in characterizing tissue damage due to the use of HIFU in thermal necrosis mode.

(3) A better understanding of tissue damage due to mechanical effects (e.g., cavitation) was achieved through careful experimental work. In particular, thresholds for the onset of cavitation under different conditions *in vivo* were measured (3). Fortunately, over the frequency range of interest for therapeutic ultrasound and normal tissue conditions, these thresholds are well above the intensity levels commonly used in thermotherapy. That is, it is possible to perform therapeutic procedures leading to tissue necrosis based on thermal effects while avoiding mechanical effects (3). Furthermore, recent research results by Umemura and coworkers (6) indicate that, with the use of appropriate pharmaceutical agents and asymmetrical pressure pulses, it is possible to significantly reduce the thresholds for cavitation and produce purely cavitational tissue necrosis.

As a result of the better understanding of the thermal and mechanical modes of tissue damage by HIFU, it is now possible to define precise therapeutic goals for various thermotherapies. There is now mounting experimental evidence that such quantitative characterization is justified and is clinically feasible.

In this article, we discuss the current status and future directions in the therapeutic use of HIFU with special emphasis on thermotherapy. After a brief discussion of the modes of interaction of HIFU with *in vivo* tissue, we address some of the latest research on the various aspects of image-guided HIFU systems for therapy. In particular, new phased array systems for precise formation of HIFU beams, noninvasive two-dimensional temperature feedback, and methods for image guidance will be addressed. In addition, some of the future directions in the use of duplex (combined imaging and therapy transducers) systems will be discussed.

In writing this article, every effort has been made to cite all relevant work published in this area. However, we recognize the difficulty of achieving completeness in this regard. It is hoped that the scope of the paper and the citations will provide the reader with a good appreciation of the fundamental bases as well as the various applications of therapeutic ultrasound. The discussion of the various topics presented in this article will be nonmathematical, but adequate technical description and citation of mathematical results will be provided for the interested reader. The use of figures and illustrations from the authors' current and previous work is simply a matter of convenience and availability at the time of writing. It should not be interpreted as a judgment on our part as to the merit of our work relative to that of others with similar interests.

The rest of this article is organized as follows. In the next section we discuss the therapeutic effects of HIFU and its interaction mechanisms with *in vivo* mammalian tissue. The third section discusses materials and methods for generation and characterization of HIFU, including quality assurance issues. The fourth section addresses some of the current challenges towards successful clinical applications of therapeutic ultrasound. This section sets the stage for the following material on noninvasive temperature feedback, image guidance, and duplex systems. Invasive and noninvasive methods for temperature feedback will be addressed in the fifth section. In the sixth we discuss image guidance of HIFU applicator systems, with special emphasis on MRI and ultrasound. Some of the future directions in the use of HIFU will be addressed in the seventh section. Concluding remarks are given in the final section.

Therapeutic Effects

It is now widely accepted that HIFU interacts therapeutically with *in vivo* tissue either thermally or mechanically or through a combination of these two effects. Thermotherapies, as the name implies, are based on the thermal interaction while eliminating or at least minimizing mechanical interactions. Thermal interactions are classified into hyperthermia, tissue coagulation, and ablation, depending on both the temperature and

duration of the heating field. Mechanical interactions are generally produced by nonlinear phenomena and can, in extreme cases, cause hemorrhage and tissue necrosis.

Thermal interactions between HIFU and *in vivo* tissues are fairly well understood. Several thermotherapeutic procedures are now in use clinically with well-defined treatment objectives. Mechanical interactions, on the other hand, are much less well understood. This has not prevented them from being put to good use, as in the case of lithotripsy. However, much more work needs to be done before controlled mechanical damage of *in vivo* tissues can be achieved clinically (4). For that reason, this article will emphasize the thermotherapeutic aspects of HIFU (but adequate reference for other therapies will be made).

Thermotherapy with High-Intensity Focused Ultrasound.

Hyperthermia. In hyperthermia, the objective is to elevate and maintain the tumor temperature to a therapeutic level of 42° to 45°C for 30 min to 60 min. Hyperthermia is not designed to produce irreversible damage to the target tissue. It produces reversible changes in tissue state that sensitize the tumor cells to other therapeutic modalities, such as radiation therapy (1, 11, 12). HIFU intensities below 100 W/cm^2 at frequencies above 500 kHz have been used in hyperthermia. At these intensity levels, cavitation was rarely reported as a treatment-limiting factor. Patient pain due to bone heating and/or excessive heating of skin and other critical tissues was encountered frequently. For a good review on ultrasound hyperthermia, the interested reader should refer to Ref. 13.

It should be noted that there is a lack of interest in hyperthermia among most researchers investigating therapeutic applications of HIFU today. This is due to continued disappointing clinical results that failed to show the synergistic effect of using hyperthermia in conjunction with radiation therapy. Most active research groups are interested in investigating the potential for direct localized tissue necrosis using HIFU. Most of the work reported in the literature today describes the use of HIFU in performing ablative or coagulative thermal surgery (4).

Thermal Surgery with HIFU. It has been verified experimentally (10) that the lesion size and shape are well predicted by the thermal dose parameter of *equivalent minutes at 43°C*, defined as

$$T_{43}(\boldsymbol{r}, t) = \int_0^t R^{T_{(\boldsymbol{r},t)}-43}\, d\tau \qquad (1)$$

where $T$is temperature in degrees Celsius, t is time in minutes, $\boldsymbol{r}$ is the radius vector in the three-dimensional coordinate system of the region of interest, and R is an empirically determined constant. Equation (1) is derived from cell survival rates at different temperatures (9). An obvious implication of Eq. (1) is that the same therapeutic endpoint (e.g., thermal coagulation) can be reached (assuming $R = 2$) by maintaining a tissue temperature of 43°C for 120 min or, alternatively, maintaining tissue temperature of 56°C for 1 s. While the two alternatives mentioned are indeed equivalent for nonlocalized heating of nonperfused tissue, they differ greatly when localized heating of perfused tissue is considered. In the case of long-duration heating, heterogeneous blood perfusion and thermal conductivity of tissue complicate the requirements of temperature control algorithms, even with the most advanced applicators. On the other hand, the short-duration heating causes thermal coagulation before blood perfusion and conduction begin to affect the heating pattern. In the latter case, the temperature control problem is reduced to a pattern synthesis problem, thus significantly simplifying the therapeutic procedure to achieve the desired endpoint. This conclusion, which is derived from theoretical analysis of the bioheat transfer equation (BHTE), is supported by a significant volume of research that has been performed for the determination of both thermal and cavitational thresholds for damage. This work, which was performed on exposed organs of small animals, indicates that thermal coagulation of tissue occurs according to a well-defined intensity–exposure relationship

$$IT_e^{0.5} = K \qquad (2)$$

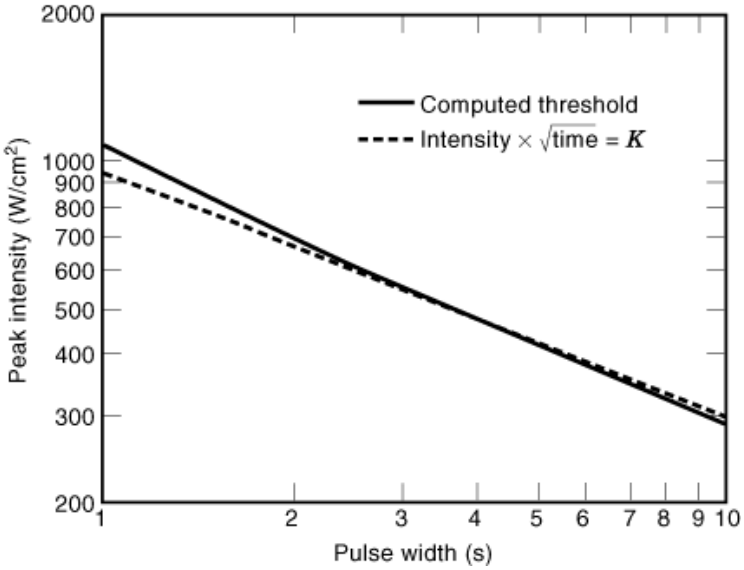

Fig. 1. Simulation of the threshold for lesion formation for exposure durations between 1 and 10 s. Solid line shows the computed intensity threshold for tissue necrosis based on Eq. (1) assuming $T_{43} = 240$ min. Dashed line shows $IT^{0.5}{}_{e} = 930$ (W/cm^2·s$^{0.5}$ based on the experimental results (2).

where I is the intensity in watts per square centimeter, T_e is the exposure (time duration) in seconds, and K is a constant depending on tissue type (3, 14, 15). For example, in Ref. 14, the cat liver threshold curve (at 3 MHz) was given by $IT^{0.5}{}_{e} = 460$ (W/cm^2)·s$^{0.5}$ for exposure durations between 0.1 s and 10 s. Interestingly enough, our thermal simulations based on the transient bioheat transfer equation (16, 17) indicate that there is general agreement between Eqs. (1) and (2) for exposure durations between 1 s and 10 s. This is illustrated in Fig. 1. Therefore, current knowledge on thermal coagulation of tissue using HIFU allows us to state the following: If one is able to control the ultrasonic power deposition for a specified time duration at a given site deep in the tissue, then thermal necrosis will occur at all points within the volume reaching the ultrasonic threshold given by Eq. (2). Equivalently, tissue damage will occur at all points within the volume reaching a thermal dose threshold given by Eq. (1).

This statement provides the basis for localized thermal surgery with HIFU. It also provides a valuable treatment planning tool for the optimization of the power deposition to the target tissue (18,19,20).

Nonthermal HIFU–Tissue Interactions. By its very nature, ultrasound is a mechanical wave phenomenon that interacts with the tissue mechanically when finite-amplitude sound waves propagate into tissue media. Mechanical interactions are primarily due to nonlinear phenomena that lead to measurable effects such as radiation pressure and streaming. These effects have been utilized to disrupt vitreous membranes, to disperse vitreous hemorrhage, and to remove detached retinas within the eye (21).

However, the most serious effect is due to nonlinear oscillations of gas bubbles that lead to the phenomenon known as transient cavitation. Transient cavitation results from the development and abrupt collapse of gaseous bubbles. It involves the formation of vapor-filled bubbles during the negative-pressure part of the acoustic cycle. During the high-pressure part of the cycle, these bubbles collapse, producing extremely high local temperatures and pressures capable of producing mechanical and chemical changes in the tissue. If uncontrolled, cavitation can cause unpredictable damage and hemorrhage (as it tends to occur near blood vessels). Thresholds for cavitation have been measured at frequencies and intensity levels relevant for both hyperthermia and thermal surgery (3). It is generally accepted that (in the absence of cavitation nuclei, e.g.,

gas bubbles and certain chemical compounds) cavitation thresholds are well above the thresholds for thermal damage. If such nuclei are present, cavitation can be achieved at considerably lower intensity levels. This is the basis for a new cancer treatment modality called sonodynamic therapy (5). Recently, Umemura and coworkers have used the method of second-harmonic superimposition (6) to produce controlled cavitation at intensity levels well below the thresholds for thermal damage *in vivo*. Other therapeutic applications of cavitation include vascular occlusion of veins, first suggested by Delon-Martin et al. (22) and later demonstrated by Hynynen et al. 23 and Rivens et al. 24.

One of the most widely used modes of mechanical interaction of HIFU with tissue is in extracorporeal shock-wave lithotripsy (*ESWL*). A lithotripter is a device that uses focused shock waves to break kidney and gall stones (25). The patient is suspended in a water bath such that the stones are positioned at the focus of the shock wave generator. Up to a thousand shocks, each on the order of 1 μs and with positive peak pressure of 50 MPa to 80 MPa, are delivered for complete destruction of the stone. Since its introduction in 1980, this procedure has been used in approximately 85% of all cases of renal stones (26). The exact roles of the mechanical effects leading to stone destruction are not well understood at this time. However, cavitation is known to play a role (27). Other possible mechanisms include pressure gradients and shear forces due to absorption and internal reflection of the incident shock wave (28).

High-Intensity Focused Ultrasound

It has been demonstrated that thermal coagulation of tissue results from short (1 s to 10 s) exposure to intense (1 kW/cm^2 to 3 kW/cm^2) acoustic fields. Furthermore, at these exposure levels and time durations, the coagulated tissue volumes are largely defined by the specific absorption rate (SAR) of the focused ultrasonic field, that is, the focal spot. For most practical ultrasound focusing systems, the coagulated tissue is cigar-shaped at the focal spot with a diameter on the order of 1 mm to 2 mm and length on the order of 3 mm to 10 mm (depending on the operating frequency and the transducer geometry). Figure 2(a) shows four lesions produced by a 1.44 MHz spherical shell piezoelectric transducer with a radius of curvature of 62.5 mm [high-power PZT-8, Etalon, Inc.—Fig. 2(b)] (29). Four 5 mm long lesions were formed by using (approximately) the same *in situ* intensity and varying the exposure duration. A large marker lesion was placed at 70 mm using a 30 s exposure for inspection purposes. The four small lesions were produced at 87 mm to 99 mm in lateral steps of 4 mm while decreasing the exposure time from 12 s to 8 s. The small axial shift in the lesion locations was intentionally produced to assess the depth resolution in the lesion formation process for the transducer. It is interesting to note that the marker and the two leftmost lesions exhibit damage patterns indicative of ablation (tissue temperature reaching the boiling point). The two rightmost lesions, on the other hand, exhibit damage patterns indicative of coagulation (peak tissue temperature below the boiling point). This coagulative mode of lesion formation by HIFU is preferred over the ablative mode (1, 30). Even higher definition of the coagulated volume can be achieved by the appropriate choice of the operating frequency and the applicator design. For example, Lizzi and coworkers (21) use a 10 MHz HIFU system in opthalmic applications.

Transducer Technologies for High-Intensity Focused Ultrasound Generation. Most HIFU systems in clinical use today employ spherical shell focused transducers operating in the range of 1 MHz through 4 MHz. High-power PZT-8 and PZT-4 piezoelectric transducer materials have been used extensively. These shell transducers are capable of producing very well-defined tissue necrosis in homogeneous tissue where no significant aberrations occur, as can be seen in Fig. 2. More recently, however, phased array applicators were developed for hyperthermia and other HIFU applications. Phased arrays offer significantly improved control features that will be needed for precision lesion formation at depth in the presence of tissue inhomogeneity and patient/applicator movement. This is due to the electronic focusing capability of these applicators, which can be performed dynamically at electronic speed to track the target (e.g., tumor) in real time for the duration of the treatment. Effects of tissue inhomogeneities can be compensated for simply by the proper choice of the phases

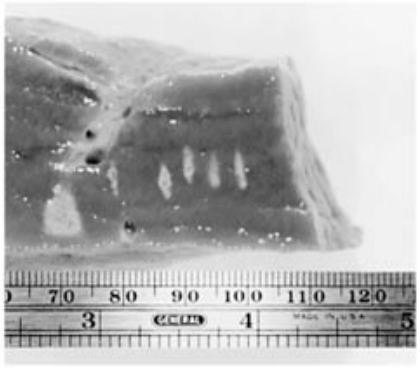

(a)

(b)

Fig. 2. (a) A series of HIFU lesions in *in vitro* calf liver. Four cigar-shaped lesions can be seen at (ruler) locations 87, 91, 95, and 99 mm, respectively. The cone-shaped lesion at ruler location 70 mm was used as a marker. (b) The transducer used in making these lesions.

of the array elements. A number of optimal phasing schemes were developed (17, 31,32,33) to refocus any array in the presence of tissue inhomogeneity, based on minimally invasive acoustic feedback using miniature probes (29, 34, 35). In addition to finding the proper phase and amplitude distribution for refocusing the array, the algorithms described in Ref. 34 identify and deactivate any elements shadowed from the target by the presence of an acoustic obstacle (e.g., bone or air spaces). More recently, a new algorithm for optimization of focused phased array patterns allowing explicitly for the rib cage has been developed (8, 36). This algorithm shows that desired focused field patterns interior to the rib cage can be realized while minimizing the direct incidence of ultrasound on the rib bone. This could eliminate one of the major problems with ultrasound and allow phased array HIFU systems to (noninvasively) target tissues previously deemed untreatable with HIFU (e.g., the liver). This algorithm may be implemented if the ribs can be imaged and taken account of in the focusing algorithm: some form of feedback on the rib geometry with respect to the array is needed. The availability of this kind of feedback will allow for the use of arbitrary array geometries with multiple acoustical windows to maximize the power deposition to the target region. Another important feature unique to phased array system is their ability to dynamically synthesize optimal multiple-focus patterns (17, 31,32,33). Multiple-focus pattern can be used to simultaneously heat multiple target points without the need for mechanical scanning. They could prove essential for the reduction of the treatment time for HIFU procedures (19, 20).

Early phased array prototypes employing relatively large elements were fabricated with PZT-8 (37). However, with the move towards 2-D arrays with larger steering capabilities, smaller array elements will be needed.

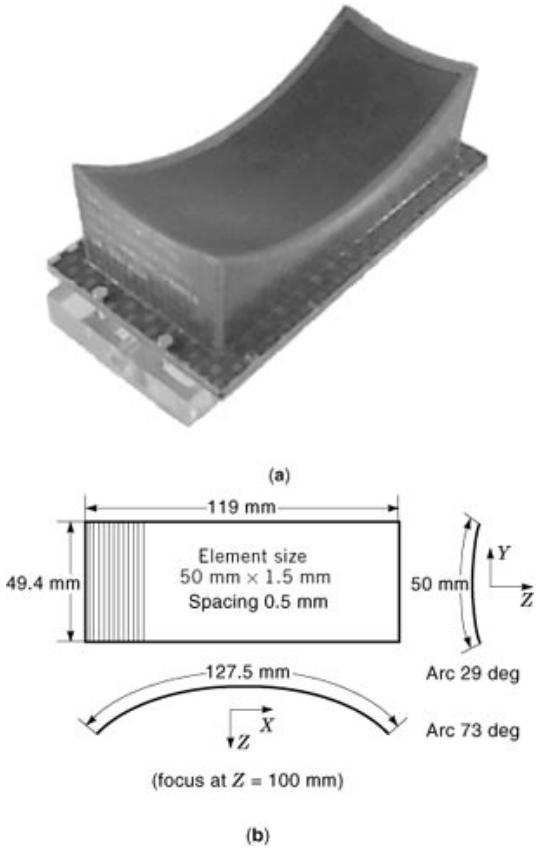

Fig. 3. 64-element piezocomposite ultrasound transducer array: (a) isometric view of applicator; (b) schematics.

This requirement proved to be challenging for conventional PZT transducer technology. This is due to the higher drive impedance of the smaller elements and increased acoustical coupling between the array elements. In addition, for small elements with surface-to-thickness ratios optimized for HIFU applications, lateral vibrational modes exist at frequencies very close to the operational thickness modes. This can significantly reduce the efficiency of the array and make it useless for HIFU applications. Fortunately, high-power, high-efficiency piezocomposite transducer materials are becoming available. This transducer technology appears to hold the promise of solving the above problems due to the fine dense discretization of the transducer aperture (38, 39). Other high-power transducer technologies are being developed and may provide further improvements in the performance of HIFU array systems. Figure 3 shows a 64-element HIFU phased array transducer fabricated with piezocomposite technology. The acoustic properties and performance characteristics of this transducer are summarized in Table 1 While the aperture size and operating frequency differ according to the application, the f number and the element size in wavelengths are typical. The fractional bandwidth of the transducer is larger than a typical air-backed PZT transducer. A higher fractional bandwidth of 60% is currently possible with piezocomposite technology. This will be extremely beneficial for duplex HIFU transducers for combined imaging and therapy (39, 40).

Modeling for High-Intensity Focused Ultrasound Therapies.

Acoustic Models. Most of the acoustic field simulations presented in the literature utilize the Rayleigh–Sommerfeld diffraction integral over an aperture in a homogeneous half space (even when simulating for

Table 1. Characteristics of a 64-element HIFU Phased Array Transducer

Center frequency	1.0 MHz
−3 dB bandwidth	37%
−3 dB focal dimension	$1 \times 2.2 \times 12$ mm^3
Max. acoustic intensity in water (focus)	5400 W/cm^2
f number	0.84

complex nonplanar array structures) (17, 41). While this model has some theoretical limitations, the experimental results indicate that it provides an adequate model for water tank measurements (34, 37, 38). Figure 4 shows 2-D cuts of the field pattern produced by the 64-element toroidal array shown in Fig. 3 at its geometric center. Experimental results are in excellent agreement with the computer simulation data shown.

Nonlinear phenomena have been modeled based on Burger's equation (42) and an incrementally linear, time-domain, finite-element model (43). It is clear that nonlinear acoustic phenomena as well as time variation in acoustic properties of tissues (due to temperature changes) should be taken into account in HIFU applications. Recent publications indicate that there is a trend among several research groups to take account of such phenomena (27, 43, 44).

Thermal Models. The BHTE introduced by Pennes (16) is probably the most widely used model for tissue temperature response to heating sources (and metabolism). Despite obvious theoretical limitations pointed out by many authors (45) for long-duration hyperthermia, it appears to be an acceptable model for lesion formation during thermal surgery (18).

Piezoelectric Models. One-dimensional piezoelectric simulation models such as the Mason and KLM models have been widely used in the literature (46). It should be pointed out, however, that 1-D simulation models for piezoelectric transducers (e.g., the KLM model) are inadequate for array elements with small width-to-thickness ratios. Two-dimensional PZT transducers designed for HIFU applications have width-to-thickness ratios on the order of 2. Finite-element models are necessary for accurate prediction of the electroacoustic behavior of such transducers. These models are reasonably accurate for transducers with width-to-thickness ratios of practical interest. Finite-element modeling of therapeutic transducers in the time (43, 47) and frequency domains (48, 49) has been reported.

Quality Assurance. Acoustic quantities related to HIFU are intensity (typically given in watts per square centimeter for hyperthermia and thermal surgery) and peak positive pressure, P^+ (typically given in megapascals). There are several useful definitions of intensity, such as the spatial-peak temporal average I_{SPTA}, spatial-peak pulse average I_{SPPA}, and spatial-average temporal average I_{SATA}. These definitions can be found in Ref. 50 In some publications on lithotripsy, the peak negative pressure P^- is also used. The ANSI 790-89 sponsored by the IEEE Ultrasonics, Ferroelectrics, and Frequency Control Society (reaffirmed in 1996) is an excellent reference on standards in medical ultrasound, including therapeutics (51). This standard describes procedures for measuring ultrasonic field parameters such as pressure, power, and intensity at various levels covering diagnostic to therapeutic applications. The most commonly used quantitative methods for acoustical measurements are hydrophone measurements (for pressure and intensity) and force balance meters (for acoustic power from a radiating transducer). The IEEE ANSI 790-1989 also contains appendices on the detection of cavitation. Some of these methods have been successfully used *in vivo* for the detection of bubble and collapse cavitation (3).

Methods for visualizing ultrasonic beams using schlieren optics (52, 53) have been developed. In addition, other imaging methods such as ultrasound (54) and magnetic resonance imaging (*MRI*) (55) are capable, in principle, of imaging the displacements due to HIFU fields.

Unlike the diagnostic ultrasound area, standard tissue-mimicking phantoms for characterizing the performance of systems for therapeutic ultrasound are virtually nonexistent. Some early attempts to establish a

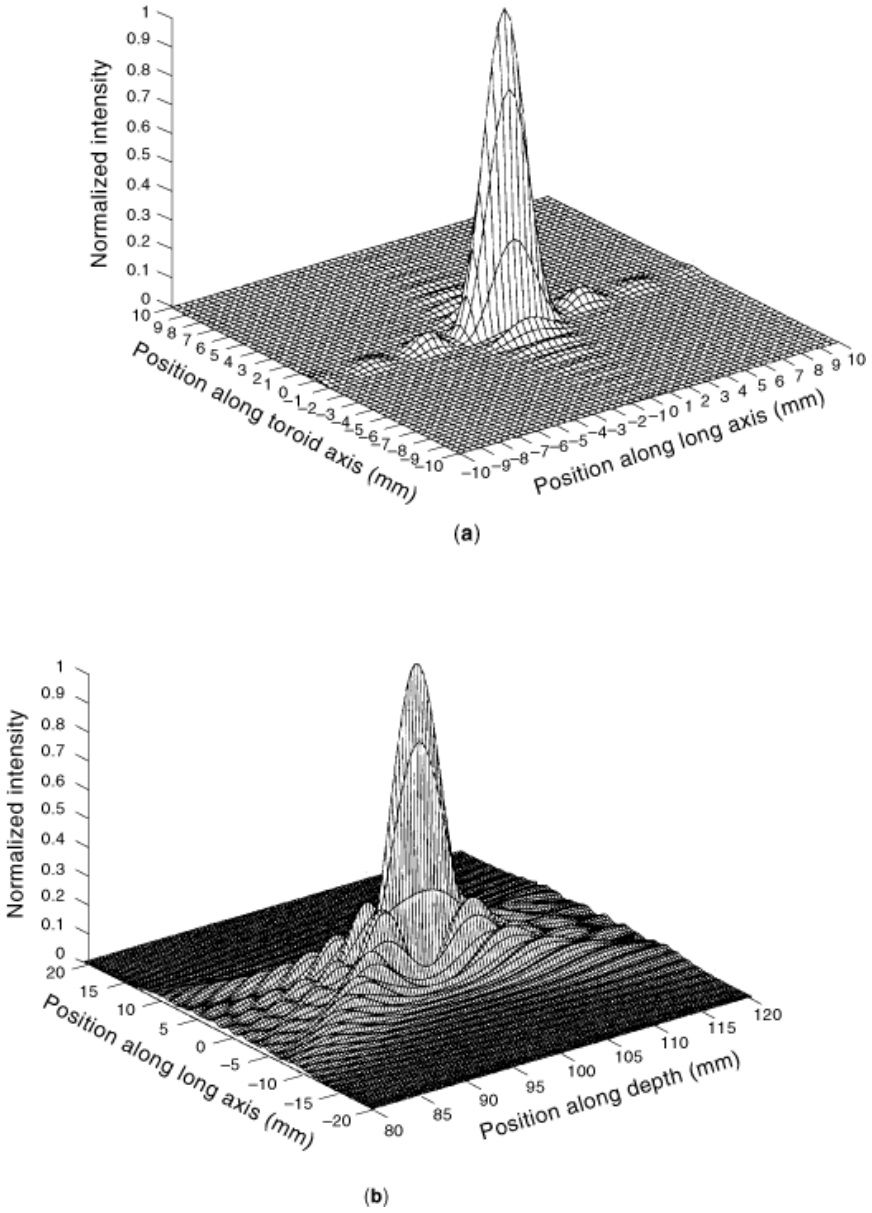

Fig. 4. Simulated intensity profiles of the geometric focus of the 64-element toroidal array: (a) *xy* plane; (b) *xz* plane. The effective dimension of the focal spot are 1 mm, 2 mm, and 12 mm in the *x, y*, and *z* directions, respectively.

standard phantom for lithotripsy are described in Ref. 56 According to Ref. 56, standard ESWL phantoms are being used by several European manufacturers today, and the trend towards standardization is encouraging. For thermotherapy, some attempts were made to utilize perfused kidney models (57) and tissue-equivalent phantoms (58). However, these phantoms were used on a very limited basis, and no effort to set standards for phantoms was made. There is a definite need for developing standard tissue-mimicking phantoms for

HIFU thermotherapies. With standard well-characterized phantoms, it may become possible to use some of the temperature imaging methods mentioned above for quantitative 2-D and 3-D intensity measurements.

Current Challenges

Despite the obvious advantages of HIFU for noninvasive therapeutic application and the availability of advanced phased-array applicator systems capable of precision lesion formation at depth, HIFU is not yet a widely accepted modality in the clinic either for normal hyperthermia or for surgery. Some of the main reasons behind this lack of progress in clinical utilization of HIFU are as follows:

(1) Lack of appropriate transducers to generate HIFU to adequately heat specified volumes (e.g., tumors) at depth in the presence of tissue inhomogeneities and/or shadowing bone structures
(2) Lack of clinical real-time noninvasive high-resolution temperature feedback throughout the treatment volume
(3) Lack of quantitative noninvasive measurement of tissue response to HIFU fields (especially important for thermal surgery). That is, we still do not have a noninvasive measurement for determining if a desired therapeutic endpoint has been reached, nor do we have a noninvasive means for measuring thresholds for irreversible tissue thermal damage *in vivo*
(4) Lack of realistic treatment planning software based on patient-specific 3-D data sets to help in the optimization of the applicator and the treatment strategy

The availability of high-power piezocomposite transducer technology will certainly be the answer to the first problem. It is safe to say that phased arrays will be utilized in precision lesion formation even in the presence of strongly scattering obstacles (e.g., the rib cage) (36). Solving the second and third problems will lead to a guidance and visualization mechanism for the therapeutic beams based on a well-established imaging modality. This may be considered the enabling technology that will finally help HIFU surgery gain widespread acceptance by the medical community. This fact has been recognized by a number of investigators with significant clinical support (59, 60). At this point, MRI (59) and B-scan ultrasound (60) are being used. These two methods (especially MRI) clearly demonstrate that guidance visualization of the effects of therapeutic beams is feasible. In addition, X-ray computed tomography (CT) has been suggested as an imaging modality suitable for monitoring HIFU treatments (61). Realistic treatment planning will depend on advances in 3-D acquisition of image data sets reflecting the thermal and acoustic properties of tissue. This is only partially accomplished with existing MRI and X-ray CT imaging systems. It should be noted, however, that if the second and third problems are effectively solved, then the fourth problem becomes a less critical one.

Temperature Feedback

Temperature feedback during hyperthermia treatments with HIFU is primarily obtained using a limited number of thermocouples placed strategically throughout the treatment volume (62). Thermocouples are inexpensive, are durable, and provide consistent temperature measurements if used appropriately. The main disadvantages in the use of thermocouples are invasiveness, limited number of temperature measurement points, uncertainty in sensor locations, and self-heating antifacts (63). Some solutions to the limitations of thermocouple-based temperature feedback are addressed in Refs. 62 and 64 However, the need for thermocouples in order to obtain temperature feedback remains one of the most difficult aspects of administering hyperthermia. Clearly a noninvasive means of temperature measurement (or estimation) is highly desirable.

In fact, in noninvasive thermal surgery, the use of thermocouples for temperature feedback in a clinical setting is not considered an option.

Recent results from a number of research groups have suggested the use of MRI (59), X-ray CT (65), impedance tomography (66), microwave radiometry (67), and backscattered ultrasound (29, 68, 69) for noninvasive temperature estimation. Each of these techniques has its particular advantages and limitations. Briefly, MRI has high sensitivity to temperature variations, which can be measured through standard T_2 -weighted images (70) or through the chemical shift (71). Some of its limitations are expense, incompatibility issues, and tradeoffs between signal-to-noise ratio and data acquisition speed. X-ray CT may be less sensitive than MRI, but may be easier to integrate with HIFU systems in most cases. Impedance tomography also has high sensitivity but suffers from low spatial resolution. Microwave radiometry is still at the early stages of development, but may offer some advantages over impedance tomography.

The remainder of this section will be devoted to noninvasive temperature estimation using beamformed RF data from commercially available ultrasound scanners (38, 54, 72). The major advantages of using ultrasound are: (1) relatively low cost, (2) real-time data collection and signal processing, (3) deep penetration inside the body, (4) good spatial and temporal localization, and (5) compatibility with the ultrasound technology used for generating the therapeutic beam. Among the ultrasound techniques, different approaches have been suggested to estimate temperature changes: analysis of the frequency-dependent attenuation (68), backscattered power (73), and speed of sound and thermal expansion (29, 38, 72).

When a region of tissue is heated, the backscattered ultrasound RF echo from this region experiences time shifts. These are caused by thermally induced local changes in the speed of sound (74) and thermal expansion in the heated region (29, 72). In Ref. 72 temperature-change estimation along one dimension was achieved by tracking the frequency variation of the echo components in the spectral domain, the echo spectrum being estimated using an autoregressive (AR) model. Some of the difficulties posed by that technique include: (1) the choice of the AR model order and (2) the need to have two or more scattering centers per window.

A new algorithm that solved these two difficulties was independently proposed by Moreno et al. (75,76,77) and 69, 78). This algorithm is based on tracking the echo time shifts in the time domain. In Refs. 69 and 78 the time-shift estimates are differentiated along the axial direction to obtain estimates of the temperature change along one dimension. In order to filter the spatial noise usually present in the time-shift estimates, a polynomial fit was used (69, 78). However, the final estimates depend on the choice of the polynomial order, therefore requiring some *a priori* knowledge of the temperature profile. In Ref. 76 this method was applied to obtain temperature estimates at a single location (the therapeutic focus) *in vivo*, while in Refs. 29 and 78, a 2-D form of this algorithm was implemented by processing the RF data in an ultrasound image, one A line at a time.

The work described in Ref. 54 extends the technique introduced in Refs. 29,69, and 72 to a 2-D temperature-change estimation technique and offers a quantitative analysis of its capabilities and limitations. In order to regularize the time-shift estimates, a separable 2-D finite impulse response (FIR) filter is used to perform spatial band-limited differentiation along the axial direction and low-pass filtering along the lateral direction. This filter controls the tradeoff between the spatial resolution and the level of ripple in the temperature estimates, being designed according to the application. Applications of the noninvasive 2-D technique presented in Ref. 54 include temperature monitoring during hyperthermia (79) and guidance for high-intensity focused ultrasound at subthreshold intensity levels. The latter includes two different aspects of interest: real-time image guidance of the location of the focal beam (38), and assessment of the quality (sharpness) of the therapeutic focus.

Image Guidance

The use of 3-D MRI and/or CT has become routine in recent years for planning surgeries. Surface and volume rendering techniques for visualization are currently well developed and allow for unprecedented views of

patient anatomy. Moreover, modern computer workstations are capable of interactive manipulation of these 3-D data sets. It has therefore become possible for surgeons to plan their procedures based on accurate mapping of the treatment volume. More recently, techniques for multimodal image guidance for neurosurgery have been proposed (80,81,82). These techniques will allow surgeons to bring their pretreatment plans to the operating room (OR). Such advances will undoubtedly help minimize patient risk in delicate surgical procedures. They could also prove beneficial in eliminating unnecessary procedures and reducing side effects of certain surgical procedures. The increasing power and falling cost of computer and visualization technology will probably be an important factor in helping image-guided surgery gain widespread acceptance in the foreseeable future. While neurosurgery is currently the major application area, it is expected that image guidance will be utilized in other surgical applications, e.g., image-guided biopsy and focused therapeutic procedures applied in tumor ablation (82).

For minimally invasive procedures, image guidance is essential for (1) identifying the target lesion, (2) planning the minimally invasive approach, and (3) monitoring the therapy as it progresses (83). MRI is ideally suited for lesion identification and planning purposes. It is less suited for real-time monitoring and may present compatibility problems for some procedures. Ultrasound, on the other hand, has excellent real-time imaging capabilities. The advent of free-hand ultrasound 3-D imaging systems makes ultrasound very attractive for treatment planning as well. However, ultrasound does not have the soft-tissue contrast needed for lesion detectability. This is the main limitation of ultrasound as an image guidance modality. Both MRI and ultrasound are nonionizing and in that respect are more attractive than other imaging techniques such as X-Ray CT.

There is little doubt that MRI is currently the most attractive imaging modality for guidance of HIFU thermotherapies. The work performed at Brigham and Women's Hospital (59, 83, 84) clearly demonstrates the capabilities of this approach. The advent of new MRI configurations such as the 0.5 T vertical access system at Brigham and Women's Hospital (83) will certainly improve the utility of MRI in image guidance.

The use of ultrasound for image guidance is much more limited and is currently confined to the use of B-scan images. Thermal coagulation of *in vivo* and *in vitro* tissues can be visualized on commercial B-scan images as an increase in the echogenicity of the coagulated tissue (60). However, gray-scale images neither precisely define the extent of the coagulated tissue nor produce a quantitative measure of tissue state.

The noninvasive 2-D temperature estimation technique described in the preceding section provides an ideal tool for guiding HIFU beams in thermal surgery (38). In order to demonstrate this capability, an *in vitro* heating experiment was performed on bovine muscle. The objective was to demonstrate that qualitative estimates of the temperature rise can be used to visualize the effect of the therapeutic beam at subthreshold intensity levels in tissue media. It should be noted, however, that to obtain calibrated temperature estimates in tissue it would be necessary to first obtain a calibrated measurement of the proportionality factor k that relates the temperature change to echo stretching in the tissue. It has been reported that this factor is highly dependent on the fraction of lipid of the tissue being considered (74). Nevertheless, for the case of beam guidance alone, calibrated estimates are typically not necessary.

The setup shown in Fig. 5 was used, where the phantom was replaced with an approximately parallelepipedal $50 \times 80 \times 60$ mm^3 sample of bovine muscle tissue. The sample was cut so that the tissue fibers were perpendicular to the therapeutic and imaging beams. A copper wire was introduced in the sample along the elevational direction of the imaging transducer, to provide a marker for the guidance procedure. A gray-scale B-scan image of the tissue sample prior to any heating (0 s) is shown in the left image in Fig. 6, where the marker is seen at axial = 44 mm, lateral = 32 mm.

A low-power therapeutic focus (single focus, temporal average intensity of 51 W/cm^2 at the focus, measured in water) was applied, and its corresponding initial heating was estimated using the technique previously described. The estimated temperature map after 15 s of heating was overlaid on the original gray-scale B-scan image, to demonstrate the guidance capability of the system. Only temperature estimates above a threshold

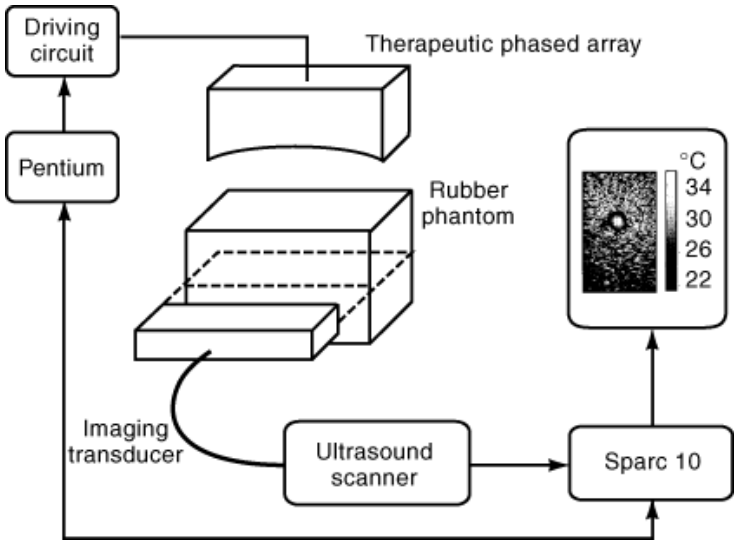

Fig. 5. Diagram of the experimental setup depicting the dual ultrasound system. This system employs a diagnostic transducer array for image guidance of the therapeutic phased array.

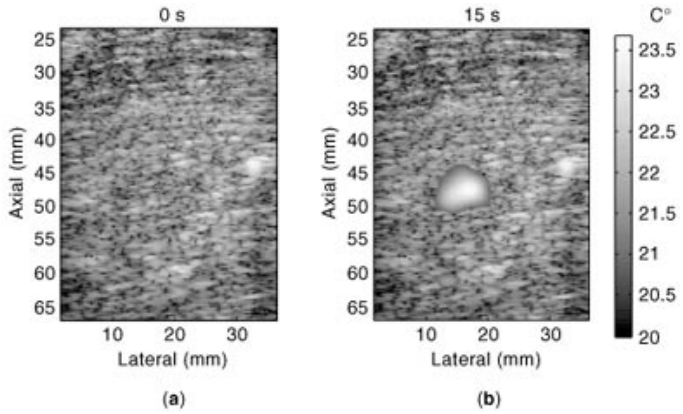

Fig. 6. Guidance for HIFU (*in vitro* tissue experiment). (a) B-scan of bovine muscle sample prior to any heating. The copper wire marker is seen at (axial = 44, lateral = 32) mm. (b) Estimated temperature map at 15 s overlaid on the B-scan image when heating at below-therapeutic power. Only temperature-change estimates above a 0.9°C threshold ($\delta\theta > 0.9$°C) are displayed. Wherever the estimated temperature is below this threshold, the underlying gray-scale B-scan image is shown.

value of 0.9°C are displayed. The temperature estimation method was capable of detecting and localizing the heating spot at axial = 47 mm, lateral = 17 mm.

A short-duration (3 s) high-power (170 W acoustic power at the surface of the therapeutic transducer) ablative pulse was then delivered at the same location, in order to form a lesion. The sample was cut, and a lesion was observed at the expected location (35 mm deep within the tissue, 15 mm to the left of and 3 mm behind the marker—Fig. 7).

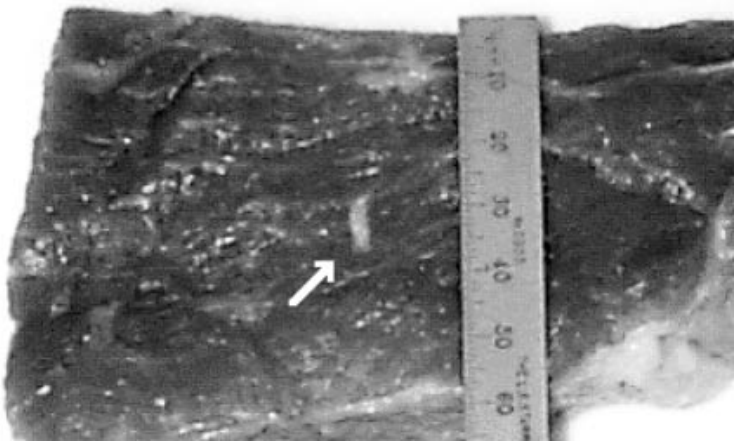

Fig. 7. Lesion found at prespecified location in bovine muscle experiment after HIFU sonication.

Future Directions

The potential of therapeutic ultrasound has not been realized yet, but its promise has never been as solid as we are experiencing nowadays. Most of the current challenges facing its clinical application have been reduced to technological challenges that will undoubtedly be solved in the foreseeable future. Advanced transducer technologies and the use of phased arrays are defining the current status of therapeutic ultrasound, both in academia and industry. Most recent publications by several active research groups indicate that the following areas might determine the future directions of therapeutic ultrasound:

- *Controlled Cavitation at Low Acoustic Intensity.* The pioneering and exciting work by Umemura and coworkers is showing strong evidence of producing controlled cavitation at intensity levels well below the thresholds for thermal damage (or even hyperthermia). Experimental results on rat liver *in vivo* demonstrate that precisely controlled tissue necrosis can be achieved and that the thresholds are due to field intensity. If successful, this approach could eliminate some of the drawbacks of thermal surgery. In particular, thermal surgery may have to be kept slow in order to avoid temperature buildup in the tissue between the applicator and the target. This is not a problem for controlled cavitation-based surgery. On the other hand, hemorrhage has been observed in lesions produced by controlled cavitation. This may be of concern when treating certain types of tumors.
- *Self-Guided Therapeutic Phased Arrays.* The use of therapeutic arrays in transmit–receive modes will allow for new methods in adaptive focusing in the presence of tissue inhomogeneity (85,86,87,88). In this approach, scattering measurements from inhomogeneous media can be used in characterizing the Green's function of the medium from the array to a desired set of control points. This allows for the use of advanced optimization techniques for control of the heating pattern at multiple locations simultaneously (17, 31,32,33, 89).
- *Duplex Arrays for Imaging and Therapy.* Many researchers considered the use of a diagnostic imaging system for guidance and monitoring of the HIFU therapy system. In most implementations, the imaging system is completely separate from the therapy system. Obviously, this will require some of form of transformation between the imaging system's coordinates and the coordinates of the HIFU therapeutic system. One solution to this problem is to integrate the imaging system into the therapy array (49). However, the

ultimate solution is to use the same therapy array for both imaging and therapy (40). In Ref. 40, it was shown that the 64-element array described in the section "Temperature Feedback" can be used to perform both imaging and therapy. This was possible due to the use of piezocomposite technology, which produced an array with approximately 37% fractional bandwidth. Even though this array was not optimized for imaging, it still produced images of adequate quality in a field of view extending nearly 7 cm by 5 cm in the axial and lateral directions with respect to the geometric center of the array. Interestingly enough, speckle data produced by this array in imaging mode were used to successfully obtain temperature images from a tissue-mimicking phantom (40).

- *Focusing in the Presence of Strongly Scattering Objects.* The use of phased arrays may allow the use of HIFU in targeting tissues that were previously considered untreatable by noninvasive focused ultrasound. For example, liver tumors are typically partially obstructed by the rib cage. This is not a problem for imaging transducers, due to their small size. However, HIFU transducers require a large aperture, which will be partially obstructed by the rib bones. The available acoustical window would be insufficient if one were to completely avoid the rib cage. On the other hand, the intercostal spacings between the rib bones provide valuable access to the target if excessive heating of the rib bones can be avoided. This problem was investigated in Refs. 8,36 and 90. As shown in Ref. 36, it is possible to focus the array in the region interior to the rib cage using a two-step algorithm. In the first step, a virtual array in the intercostal spacings is used to synthesize the desired field pattern in the area interior to the rib cage. In the second step, the actual array is used to synthesize the virtual array excitation while explicitly minimizing the direct incidence of acoustic power over the ribs. Other applications requiring similar techniques include extracardiac ablation of ventricular myocardium (91) and focusing through the skull (87).
- *Noninvasive Methods for Damage Assessment.* The ultimate success of image-guided noninvasive surgery, whether thermal or nonthermal, may hinge on the availability of noninvasive methods for assessment of tissue state. That is, can we image certain tissue properties that are indicative of whether the treated target tissue has undergone irreversible damage or reversible change? At the time of writing this article, this question has not been answered fully. Clearly, MRI and X-ray CT hold the most promise to provide the answer, due to their quantitative nature. Tissue characterization methods with ultrasound have not been successful in discriminating between normal and diseased tissue. However, the changes in tissue state due to therapeutic procedures are so drastic that some of the ultrasonic tissue characterization methods may prove useful in discriminating between normal and necrosed tissue (30, 92). Furthermore, the significant improvement in the quality of beamformed data from imaging arrays will allow for advanced signal-processing methods for feature extraction. It is fair to expect, therefore, that this area will receive a lot of attention in the near future as more data from *in vivo* HIFU experiments become available.

Conclusions

It is quite clear that research in therapeutic ultrasound over the last two decades has significantly improved our understanding of the modes of interactions between HIFU and tissue. Much better discrimination between mechanical and thermal effects is now available. In addition, noninvasive tools for measuring temperature (54) and detecting stable and transient cavitation (3) are now well developed. In addition, thresholds for thermal tissue damage have been measured (3, 14). These thresholds, along with the development of the thermal dose concept have allowed for a clear definition of the treatment objectives for noninvasive thermal surgery with HIFU (10). Furthermore, the exciting results by Umemura and coworkers (6) on sonodynamic drug activation indicate that cavitation thresholds can be lowered significantly by appropriate choice of the acoustic pulse (using the second-harmonic superimposition technique). This work shows clear promise that cavitation can be spatially controlled at moderate field intensity levels. The use of piezocomposite transducer arrays in ESWL, along with a better understanding of the role of cavitation in stone destruction (27), will probably further

improve this already successful procedure. It is clear now that both mechanical and thermal modes of HIFU–tissue interactions can be produced in a controlled manner in selected tissues. In the near future, it is very likely that systems utilizing either one mode of interaction or a combination of both will be developed to optimize the therapeutic endpoint of the treatment. The use of phased array systems and availability of noninvasive feedback will allow HIFU to noninvasively access tissue targets previously considered unreachable by ultrasound, such as liver tumors (36). Finally, image guidance through well-established medical imaging modalities (61, 83, 93) will play a key role in the clinical acceptance of most noninvasive HIFU-based therapeutic procedures that are currently being investigated.

Acknowledgments

This work was partially funded by NSF Young Investigator Award ECS 9358301 and NIH Grant CA66602.

BIBLIOGRAPHY

1. P. Lele Ultrasound: Synergistic effects and application in cancer therapy by hyperthermia, in M. Repacholi, M. Grondolfo, and A. Rindi (eds.), *Ultrasound: Medical Applications, Biological Effects and Hazard Potential*, New York: Plenum, 1987.
2. J. Hunt *et al.* Rapid heating: Critical theoretical assessment of thermal gradients found in hyperthermia treatments, *Int. J. Hyperthermia*, **7** (5): 703–718, 1991.
3. P. Lele Effects of ultrasound on "solid" mammalian tissues and tumors in vivo, in M. Repacholi, M. Grondolfo, and A. Rindi (eds.), *Ultrasound: Medical Applications, Biological Effects and Hazard Potential*, New York: Plenum, 1987.
4. K. Hynynen Review of ultrasound therapy, *IEEE Ultrason. Symp.*, pp. 1305–1313, 1997.
5. S. Umemura *et al.* Sonochemical activation if hematopophyrin: A potential modality for cancer treatment, *IEEE Ultrason. Symp.*, **2**: 955–960, 1989.
6. S. Umemura *et al.* In vitro and in vivo enhancement of sonodynamically active cavitation by second-harmonic superimposition, *J. Acoust. Soc. Am.*, **101** (1): 569–577, 1997.
7. R. Magin A. Peterson Noninvasive microwave phased arrays for local hyperthermia: A review, *Int. J. Hyperthermia*, **5** (4): 429–450, 1989.
8. Y. Botros *et al.* A hybrid computational model for ultrasound phased array heating in the presence of strongly scattering obstacles, *IEEE Trans. Biomed. Eng.*, **44**: 1039–1050, 1997.
9. S. Saparato W. Dewey Thermal dose determination in cancer therapy, *Int. J. Radiat. Oncol. Biol. Phys.*, **10**: 787–800, 1984.
10. C. Damianou K. Hynynen, X. Fan Evaluation of accuracy of a theoretical model for predicting the necrosed tissue volume during focused ultrasound surgery, *IEEE Trans. Ultrason. Ferroelectr. Freq. Control*, **42**: 182–187, 1995.
11. G. Hahn Hyperthermia for the engineer: A short biological primer, *IEEE Trans. Biomed. Eng.*, **31**: 3–8, 1984.
12. T. Samulski E. Lee, G. Hahn Hyperthermia as a clinical treatment modality, *Cancer Treat. Rep.*, **68** (1): 309–316, 1984.
13. K. Hynynen Ultrasound heating technology, in M. Seegenschmiedt, P. Fessenden, and C. Vernon (eds.), *Thermo-radiotherapy and Thermo-chemotherapy*, Berlin: Springer, 1995, pp. 253–277.
14. L. Frizzell Threshold dosages for damage to mammalian liver by high-intensity focused ultrasound, *IEEE Trans. Ultrason. Ferroelectr. Freq. Control*, **35**: 578–581, 1988.
15. W. Fry *et al.* Ultrasonic lesions in the mammalian central nervous system, *Science*, **122**: 517–518, 1955.
16. H. Pennes Analysis of tissue and arterial blood temperature in the resting human forearm, *J. Appl. Physiol.*, **1**: 93, 1948.
17. E. Ebbini Deep localized hyperthermia with ultrasound phased arrays using the pseudoinverse pattern synthesis method, Ph.D. thesis, Department of Electrical Engineering University of Illinois at Urbana-Champaign, 1990.
18. C. Damianou K. Hynynen Focal spacing and near-field heating during pulsed high temperature ultrasound therapy, *Ultrasound Med. Biol.*, **19** (9): 777–787, 1993.

19. H. Wan *et al.* Ultrasound surgery: Comparison of strategies using phased array systems, *IEEE Trans. Ultrason. Ferroelectr. Freq. Control* **43**: 1085–1098, 1996.
20. D. Daum K. Hynynen Thermal dose optimization via temporal switching in ultrasound surgery, *IEEE Trans. Ultrason. Ferroelectr. Freq. Control*, **45**: 208–215, 1998.
21. J. Driller F. Lizzi Therapeutic applications of ultrasound: A review, *IEEE Eng. Med. Biol. Mag.* **6** (4): 33–40, 1987.
22. Delon-Martin et al., Venous thrombosis generation by means of high intensity focused ultrasound, *Ultrasound Med. Biol.*, **21** (1): 113–119, 1995.
23. K. Hynynen *et al.* Noninvasive artery occlusion using MRI guided focused ultrasound, *Ultrasound Med. Biol.*, **22**: 1071–1077, 1996.
24. I. Rivens *et al.* Focused ultrasound surgery induced vascular occlusion in fetal medicine, *Proc. SPIE*, **3249**: 261–266, 1998.
25. R. Riehle *Principles of Extracorporeal Shock Wave Lithotripsy*, London: Churchill-Livingstone, 1987.
26. D. Cathignol A. Birer Beam steering for shock waves using 30 cm bidimensional array, *IEEE Ultrason. Symp.*, pp. 1801–1804, 1994.
27. D. Cathignol *et al.* Comparison between the effects of cavitation induced by two different pressure–time shock waveform pulses, *IEEE Trans. Ultrason. Ferroelectr. Freq. Control*, **45**: 788–799, 1998.
28. A. Coleman *et al.* Acoustic cavitation generated by an extracorporeal shockwave lithtripter, *Ultrasound Med. Biol.*, **13**: 69–76, 1987.
29. R. Seip Feedback for ultrasound thermotherapy, Ph.D. thesis, Department of Electrical Engineering and Computer Science, University of Michigan, Ann Arbor, 1996.
30. A. L. Macom G. R. ter Haar Ablation of tissue volumes using high intensity focused ultrasound, *Ultrasound Med. Biol.*, **22**: 659–669, 1996.
31. E. Ebbini C. Cain Multiple-focus ultrasound phased-array pattern synthesis: Optimal driving-signal distributions for hyperthermia, *IEEE Trans. Ultrason. Ferroelectr. Freq. Control.*, **36**: 540–548, 1989.
32. E. Ebbini C. Cain Optimization of the intensity gain of multiple-focus phased array heating patterns, *Int. J. Hyperthermia*, **7** (6): 953–973, 1991.
33. E. Ebbini C. Cain A spherical-section ultrasound phased array applicator for deep localized hyperthermia, *IEEE Trans. Biomed. Eng.*, **38**: 634–643, 1991.
34. R. Seip P. VanBaren, E. Ebbini Dynamic focusing in ultrasound hyperthermia treatments using implantable hydrophone arrays, *IEEE Trans. Ultrason. Ferroelectr. Freq. Control*, **41**: 706–713, 1994.
35. H. Wang *et al.* Phased aberration correction and motion compensation for ultrasonic hyperthermia phased arrays: Experimental results, *IEEE Trans. Ultrason. Ferroelectr. Freq. Control*, **41**: 34–43, 1994.
36. Y. Botros E. Ebbini, J. Volakis Two step hybrid virtual array-ray (var) technique for focusing through the rib cage, *IEEE Trans. Ultrason. Ferroelectr. Freq. Control*, **45**: 989–1000, 1998.
37. E. Ebbini C. Cain Experimental evaluation of a prototype phased array applicator, *IEEE Trans. Ultrason. Ferroelectr. Freq. Control*, **38**: 510–520, 1991.
38. P. VanBaren *et al.* Image-guided phased array system for ultrasound thermotherapy, *IEEE Ultrason. Symp.*, pp. 1269–1272, 1996.
39. G. Fleury *et al.* New piezoelectric transducers for therapeutic ultrasound, *Ultrasound Med. Biol.*, 1998, submitted for publication.
40. C. Simon *et al.* Combined ultrasound image guidance and therapy using a therapeutic phased array, *Proc. SPIE*, 1998.
41. K. Hynynen *et al.* A scanned, focused, multiple-transducer ultrasonic system for localized hyperthermia treatments, *Int. J. Hyperthermia*, **3** (1): 21–35, 1987.
42. W. Swindell A theoretical study of nonlinear acoustic effects with focused ultrasound in tissue: An acoustic Bragg peak, *Ultrasound Med. Biol.*, **6** (1): 345–357, 1985.
43. G. Wojcik *et al.* Nonlinear modeling of therapeutic ultrasound, *IEEE Ultrason. Symp.*, pp. 1617–1622, 1995.
44. P. Meaney *et al.* The intensity dependence of focused ultrasound lesion position, *Proc. SPIE* **3249**: 246–256, 1998.
45. H. Brinck J. Werner Use of vascular and non-vascular models for the assessment of temperature distributions during induced hyperthermia, *Int. J. Hyperthermia*, **11**: 615–626, 1994.
46. G. Kino *Acoustic Waves: Devices, Imaging, and Analog Signal Processing*, Englewood Cliffs, NJ: Prentice-Hall, 1987.
47. N. Abboud *et al.* Finite element modeling of ultrasonic transducers, *Proc. SPIE* **3341**: 19–42, 1998.

48. T. Sheljaskov *et al.* A phased array antenna for simultaneous HIFU therapy and sonography, *IEEE Ultrason. Symp.*, pp. 1527–1530, 1996.
49. T. Sheljaskov *et al.* A phased array antenna for simultaneous thermotherapy and sonography, *IEEE Ultrason. Symp.*, 1997.
50. National Council on Radiation Protection and Measurements, *Exposure Criteria for Medical Diagnostic Ultrasound. I. Criteria Based on Thermal Mechanisms: Recommendations of the National Council on Radiation Protection and Measurements*, Tech. rep. 113. Bethesda, MD: NCRP, 1992.
51. IEEE Web Site on Standards: http://standards.ieee.org/ (Search for Ultrasound)
52. A. Hanafy C. A. Zanelli Quantitative realtime pulsed schlieren imaging for ultrasonic waves, *IEEE Ultrason. Symp.*, **2**: 1223–1227, 1991.
53. T. A. Pitts *et al.* Tomographic schlieren imaging for measurement of beam pressure and intensity, *IEEE Ultrason. Symp.*, **3**: 1665–1668, 1994.
54. C. Simon P. VanBaren, E. Ebbini Two-dimensional temperature estimation using diagnostic ultrasound, *IEEE Trans. Ultrason. Ferroelectr. Freq. Control*, **45**: 1088–1099, 1998.
55. D. B. Plewes *et al.* Quantitative magnetic resonance imaging of ultrasound field, *IEEE Ultrason. Symp.*, **2**: 1353–1356, 1997.
56. U. Schätzle *et al.* Quality assurance tools for therapeutic ultrasound, *Ultrasonics*, **35**: 679–682, 1998.
57. S. D. Prionas *et al.* Flow dependence of 2d temperature distributions induced in perfused canine kidney by ultrasound, *Int. J. Hyperthermia*, **7**: 367–384, 1991.
58. IEEE, Spatial distributions of heating by ultrasound transducers in clinical use, indicated in tissue equivalent phantoms, *Proc. Ultrason. Symp.* 1985, vol. 1.
59. K. Hynynen *et al.* Feasibility of using ultrasound phased arrays for MRI monitored noninvasive surgery, *IEEE Trans. Ultrason. Ferroelectr. Freq. Control*, **43**: 1043–1053, 1996.
60. N. Sanghvi *et al.* Noninvasive surgery of prostate tissue by high-intensity focused ultrasound, *IEEE Trans. Ultrason. Ferroelectr. Freq. Control*, **43**: 1099–1110, 1996.
61. J. Jenne *et al.* CT on-line monitoring of HIFU therapy, *IEEE Ultrason. Symp.*, **2**: 1377–1380, 1997.
62. S. Clegg R. Roemer Towards the estimation of three-dimensional temperature fields from noisy temperature measurements during hyperthermia, *Int. J. Hyperthermia*, **5** (4): 467–484, 1989.
63. F. Waterman R. Nerlinger, J. Leeper Catheter induced temperature artifacts in ultrasound hyperthermia, *Int. J. Hyperthermia*, **6** (2): 371–381, 1990.
64. F. Waterman Estimation of temperature artifact from a short interruption in ultrasonic power, *Int. J. Hyperthermia*, **8** (3): 395–400, 1992.
65. B. Fallone P. Moran, E. Podgorsak Noninvasive thermometry with a clinical X-ray scanner, *Med. Phys.*, **9** (5): 715–721, 1982.
66. K. Paulsen *et al.* Initial in vivo experience with EIT as a thermal estimator during hyperthermia, *Int. J. Hyperthermia*, **12** (5): 573–591, 1996.
67. P. Meaney *et al.* Microwave imaging for tissue assessment: Initial evaluation in multitarget tissue-equivalent phantoms, *IEEE Trans. Biomed. Eng.*, **43**: 878–890, 1996.
68. S. Ueno *et al.* Ultrasound thermometry in hyperthermia, *IEEE Ultrason. Symp.*, pp. 1645–1652, 1990.
69. R. Seip *et al.* Non-invasive real-time multipoint temperature control for ultrasound phased array treatments, *IEEE Trans. Ultrason. Ferroelectr. Freq. Control*, **43**: 1063–1073, 1996.
70. D. Parker Applications of NMR imaging in hyperthermia: An evaluation of the potential for localized tissue heating and noninvasive temperature monitoring, *IEEE Trans. Biomed. Eng.*, **31**: 161–167, 1984.
71. A. Webb *et al. in vivo* NMR thermometry with liposomes containing^{59} Co, *Int. J. Hyperthermia*, **11**: 821–827, 1995.
72. R. Seip E. Ebbini Non-invasive estimation of tissue temperature response to heating fields using diagnostic ultrasound, *IEEE Trans. Biomed. Eng.*, **42**: 828–839, 1995.
73. W. Straube R. Arthur Theoretical estimation of the temperature dependence of backscattered ultrasonic power for noninvasive thermometry, *Ultrasound Med. Biol.*, **20** (9): 915–922, 1994.
74. R. Nasoni T. Bowen Ultrasonic speed as a parameter for non-invasive thermometry, in S. Mizushina (ed.), *Non-invasive Temperature Measurement*, New York: Gordon Breach, 1989, Vol. 1, pp. 95–107.
75. R. Moreno C. Damianou Noninvasive temperature estimation in tissue via ultrasound echo-shifts. Part I: Analytical model, *J. Acoust. Soc. Am.*, **100** (4): 2514–2521, 1996.

76. R. Moreno C. Damianou, N. Sanghvi Tissue temperature estimation *in-vivo* with pulse-echo, *IEEE Ultrason. Symp.*, pp. 1225–1229, 1995.
77. R. Moreno C. Damianou, N. Sanghvi Noninvasive temperature estimation in tissue via ultrasound echo-shifts. Part II: In-vitro study, *J. Acoust. Soc. Am.*, **100** (4): 2522–2530, 1996.
78. R. Seip *et al.* Non-invasive spatio-temporal temperature change estimation using diagnostic ultrasound, *IEEE Ultrason. Symp.*, pp. 1613–1616, 1995.
79. C. Simon P. VanBaren, E. Ebbini Quantitative analysis and applications of non-invasive temperature estimation using diagnostic ultrasound, *IEEE Ultrason. Symp.*, pp. 1319–1322, 1997.
80. R. Maciunas *Interactive Image-Guided Neurosurgery*, American Association of Neurological Surgeons, 1993.
81. T. Peters *et al.* Three-dimensional multimodal image guidance for neurosurgery, *IEEE Trans. Med. Imag.*, **15**: 121–128, 1996.
82. W. Grimson *et al.* An automatic registration method for frameless stereotaxy, image guided surgery, and enhanced reality visualization, *IEEE Trans. Med. Imag.*, **15**: 129–140, 1996.
83. T. Wong MR imaging guidance for minimally invasive procedures, *Proc. SPIE*, **3249**: 162–170, 1998.
84. K. Hynynen *et al.* MRI-guided non-invasive ultrasound surgery, *Med. Phys.* **20**: 107–115, 1993.
85. M. Fink *et al.* Self focusing in inhomogeneous media with time reversal acoustic mirrors, *IEEE Ultrason. Symp.*, October, pp. 681–686, 1989.
86. O. S. Haddadin E. S. Ebbini Self-focusing arrays for imaging and therapy through inhomogeneous media, *IEEE Ultrason. Symp.*, pp. 1563–1566, 1996.
87. J.-L. Thomas M. Fink Ultrasonic beam focusing through tissue inhomogeneities with a time reversal mirror: Application to transkull therapy, *IEEE Trans. Ultrason. Ferroelectr. Freq. Control*, **43**: 1122–1129, 1996.
88. O. Haddadin E. Ebbini Ultrasonic focusing through inhomogeneous media by application of the inverse scattering problem, *J. Acoust. Soc. Am.*, **104**: 313–325, 1998.
89. P. VanBaren E. Ebbini Multipoint temperature control during hyperthermia treatments: Theory and simulation, *IEEE Trans. Biomed. Eng.*, **42**: 818–827, 1995.
90. Y. Botros Optimal phased array pattern synthesis for non-invasive cancer ablation of liver tumors using high intensity focused ultrasound, Ph.D. thesis, Department of Electrical Engineering and Computer Science, University of Michigan, Ann Arbor, 1998.
91. S. Strickberger *et al.* Extracardiac application of high intensity focused ultrasound for ablation of ventricular myocardium, *Eur. J. C. P. E.*, **7** (2): 60–67, 1997.
92. M. R. Gertner *et al.* Ultrasound properties and images of ex-vivo liver during thermal therapy, *IEEE Ultrason. Symp.*, **2**: 1353–1356, 1997.
93. E. Ebbini P. VanBaren C. Simon Image-guided noninvasive surgery with ultrasound phased arrays, *Proc. SPIE* **3249**: 230–239, 1998.

READING LIST

N. Bilaniuk G. Wong Speed of sound in pure water as a function of temperature, *J. Acoust. Soc. Am.*, **93** (3): 1609–1612, 1993.

BUL Web Site on Image Guided Thermotherapy: http://bul.eecs.umich.edu/research/imageguided

R. Clarke Modification of intensity distributions from large aperture sources, *Ultrasound Med. Biol.*, **21**: 353–363, 1995.

P. Corry *et al.* Human cancer treatment with ultrasound, *IEEE Trans. Sonics Ultrason.*, **31**: 444–456, 1984.

D. Daum *et al.* Design and evaluation of a feedback based phased array system for ultrasound surgery, *IEEE Trans. Ultrason. Ferroelectr. Freq. Control*, **45**: 431–438, 1998.

C. Diederich E. Burdette Transurethral ultrasound array for prostate thermal therapy: Initial studies, *IEEE Trans. Ultrason. Ferroelectr. Freq. Control*, **43**: 1011–1022, 1996.

D. Donoho De-noising by soft-thresholding, *IEEE Trans. Inf. Theory*, **41**: 613–627, 1995.

L. Dorr K. Hynynen The effects of tissue heterogeneities and large blood vessels on the thermal exposure induced by short high-power ultrasound pulses, *Int. J. Hyperthermia*, **8** (1): 45–59, 1992.

F. Dupenloup *et al.* Reduction of the grating lobes of annular arrays used in focused ultrasound surgery, *IEEE Trans. Ultrason. Ferroelectr. Freq. Control*, **43**: 991–998, 1996.

E. Ebbini F. Ngo, C. Cain The pseudoinverse pattern synthesis method: Experimental verification using a prototype cylindrical-section ultrasound hyperthermia phased-array applicator, *IEEE Ultrason, Symp.*, pp. 995–998, 1989.

E. Ebbini, *et al.* A cylindrical-section ultrasound phased-array applicator for hyperthermia cancer therapy, *IEEE Trans. Ultrason. Ferroelectr. Freq. Control*, **35**: 561–572, 1988.

X. Fan K. Hynynen The effect of wave reflection and refraction at soft tissue interfaces during ultrasound hyperthermia treatments, *J. Acoust. Soc. Am.*, **91** (3): 1727–1736, 1992.

A. Fenster *et al.* Three-dimensional ultrasound imaging of the vasculature, *Ultrasonics*, **35**: 629–633, 1998.

T. Fjield *et al.* Design and experimental verification of the thin acoustic lenses for the coagulation of large tissue volumes, *Phys. Med. Biol.*, **42**: 2341–2354, 1997.

C. Floch M. Fink Ultrasonic mapping of the temperature distribution in hyperthermia: The thermal lens effect, *IEEE Ultrason. Symp.*, 1997.

R. Foster *et al.* High-intensity focused ultrasound in the treatment of prostatic disease, *Eur. Urol.*, **23** (Suppl. 1): 29–33, 1993.

F. Fry Intense focused ultrasound in medicine, *Eur. Urol.*, **23** (Suppl. 1): 2–7, 1993.

A. Gelet *et al.* High-intensity focused ultrasound experimentation on human benign prostatic hypertrophy, *Eur. Urol.*, **23** (Suppl. 1): 44–47, 1993.

A. Gelet *et al.* Treatment of prostate cancer with transrectal focused ultrasound: Early clinical experience, *Eur. Urol.*, **29**: 174–183, 1996.

S. Goss *et al.* Sparse random ultrasound phased array for focal surgery, *IEEE Trans. Ultrason. Ferroelectr. Freq. Control*, **43**: 1111–1121, 1996.

H. Hachiya *et al.* Determination of sound speed in biological tissues based on frequency analysis of pulse response, *J. Acoust. Soc. Am.*, **92** (3): 1564–1568, 1992.

I. Hein W. O. Jr. Current time-domain methods for assessing tissue motion by analysis from reflected ultrasound echoes—A review, *IEEE Trans. Ultrason. Ferroelectr. Freq. Control*, **40**: 84–102, 1993.

C. Hill G. terHaar Review article: High intensity focused ultrasound—potential for cancer treatment, *Br. J. Radiol.*, **68**: 1296–1303, 1995.

D. Hughes B. Snyder Speed of 10 MHz sound in canine aortic wall: Effects of temperature, storage and formaline soaking, *Med. Biol. Eng. Comput.* **18**: 220–222, 1980.

E. Hutchinson K. Hynynen Intracavitary ultrasound phased arrays for noninvasive prostate surgery, *IEEE Trans. Ultrason. Ferroelectr. Freq. Control*, **43**: 1032–1042, 1996.

K. Hynynen *et al.* Ultrasound phased arrays for noninvasive surgery and therapy, *SPIE Med. Imag. Symp.*, pp. 84–88, 1998.

K. Hynynen *et al.* Errors in temperature measurement by thermocouple probes during ultrasound induced hyperthermia, *Br. J. Radiol.*, **56**: 969–970, 1983.

K. Hynynen *et al.* Thermal effects of focused ultrasound on the brain: Determination with MR imaging, *Radiology*, **204**: 247–253, 1997.

K. Kuroda *et al.* Temperature mapping using the water proton chemical shift: A chemical shift selective phase mapping method, *Magn. Reson. Med.*, **38**: 845–851, 1997.

R. Lalonde J. Hunt Variable frequency field conjugate lenses for ultrasound hyperthermia, *IEEE Trans. Ultrason. Ferroelectr. Freq. Control*, **42**: 825–831, 1995.

R. Lalonde A. Worthington, J. Hunt Hyperthermia: Field conjugate acoustic lenses for deep heating, *IEEE/EMBS Conf.*, Philadelphia, pp. 235–236, 1990.

C. Linke *et al.* Localized tissue destruction by high-intensity focused ultrasound, *Arch. Surg. (Chicago)*, **107**: 887–891, 1973.

F. Lizzi *et al.* Ultrasonic hyperthermia for ophthalmic therapy, *IEEE Trans. Sonic Ultrason.*, **31**: 473–481, 1984.

T. Loupas J. Powers, R. Gill An axial velocity estimator for ultrasound blood flow imaging, based on a full evaluation of the Doppler equation by means of a two-dimensional autocorrelation approach, *IEEE Trans. Ultrason. Ferroelectr. Freq. Control*, **42**: 672–688, 1995.

R. McGough *et al.* Treatment planning for hyperthermia with ultrasound phased arrays, *IEEE Trans. Ultrason. Ferroelectr. Freq. Control*, **43**: 1074–1084, 1996.

P. Meaney K. Paulsen, T. Ryan Microwave thermal imaging using a hybrid element method with a dual mesh scheme for reduced computation time, *Proc. IEEE Conf. Eng. Med. Biol.*, pp. 96–97, 1993.

W. Moore *et al.* Evaluation high-intensity therapeutic ultrasound irradiation in the treatment of experimental hepatom, *J. Pediatr. Surg.*, **24** (1): 30–33, 1989.

R. Nasoni *et al. In vivo* temperature dependence of ultrasound speed in tissue and its application to noninvasive temperature monitoring, *Ultrason. Imag*, **1** (1): 34–43, 1979.

A. Oppenheim R. Schafer *Discrete-Time Signal Processing*, Englewood Cliffs, NJ: Prentice-Hall, 1989.

K. Paulsen M. Moskowitz, T. Ryan Temperature estimation using electrical impedance profiling methods: I. Reconstruction algorithm and simulated results, *Int. J. Hyperthermia*, **10**: 209–228, 1994.

J. Poorter *et al.* Noninvasive MRI thermometry with the proton resonance frequency (PRF) method: In vivo results in human muscle, *Magn. Reson. Med.*, **33**: 74–81, 1995.

N. Sanghvi *et al.* Preliminary findings of treatment of canine prostatic tissue using high-intensity focused ultrasound, *J. Ultrasound Med.*, **10**: s45, 1991.

M. Sapozink The application of thermal dose in clinical trials, *Int. J. Hyperthermia*, **2** (2): 157–164, 1986.

J. Shen E. Ebbini A new coded-excitation ultrasound imaging system. Part II: Operator design, *IEEE Trans. Ultrason. Ferroelectr. Freq. Control*, **43**: 141–148, 1996.

J. Shen *et al.* A post-beamforming processing technique for enhancing conventional pulse-echo ultrasound imaging contrast resolution, *IEEE Ultrason. Symp.*, pp. 1319–1322, 1995.

C. Simon *et al.* A robust and computationally efficient algorithm for mean scatterer spacing estimation, *IEEE Trans. Ultrason. Ferroelectr. Freq. Control*, **44**: 882–894, 1997.

C. Simon P. VanBaren, E. Ebbini Motion compensation algorithm for non-invasive two-dimensional temperature estimation using diagnostic pulse-echo ultrasound, *Proc. SPIE*, 1998.

V. Singh *et al.* Ultrasonic velocity as a noninvasive measure of temperature in biological media, *Appl. Acoust.*, **29**: 73–80, 1990.

L. Sullivan *et al.* Early experience with high-intensity focused ultrasound for the treatment of benign prostatic hypertrophy, *Br. J. Urol.*, **79**: 172–176, 1997.

M. Tanter J. Thomas, M. Fink Focusing through skull with time reversal mirrors: Application to hyperthermia, *IEEE Ultrason. Symp.*, pp. 1289–1293, 1996.

G. terHaar *et al.* High intensity focused ultrasound for the treatment of rat tumors, *Phys. Med. Biol.*, **36** (11): 1495–1501, 1991.

K. Thomenius Evolution of ultrasound beamformers, *IEEE Ultrason. Symp.*, pp. 1615–1622, 1996.

P. VanBaren Multipoint temperature control using therapeutic phased array ultrasound applicators with invasive and non-invasive temperature measurements, Ph.D. thesis, Electrical Engineering and Computer Sci. Department, University of Michigan, Ann Arbor, 1998.

T. Varghese K. Donohue Estimating mean scatterer spacing with the frequency-smoothed spectral autocorrelation function, *IEEE Trans. Ultrason. Ferroelectr. Freq. Control*, **42**: 451–463, 1995.

W. Walker G. Trahey Aberrator integration error in adaptive imaging, *IEEE Trans. Ultrason. Ferroelectr. Freq. Control*, **44**: 780–791, 1997.

EMAD S. EBBINI
University of Minnesota
RALF SEIP
Focus Surgery
PHILIP VANBAREN
Vibration Research
OSAMA HADDADIN
ATL Ultrasound
CLAUDIO SIMON
ATL Ultrasound
YOUSSRY Y. BOTROS
Intel